

Supporting Information to

Quantitative Assessment of Molecular Transport through Sub-3 nm Silica Nanochannels by Scanning Electrochemical Microscopy

Lina Yao^{a,b}, Fraser P. Filice^b, Qian Yang^a, Zhifeng Ding^{*b}, Bin Su^{*a}

^a Institute of Analytical Chemistry, Department of Chemistry, Zhejiang University, Hangzhou 310012, China

^b Department of Chemistry, Western University, London N6A 5B7, Canada

* Corresponding Authors:

Prof. Zhifeng Ding, Email: zfding@uwo.ca

Prof. Bin Su, Email: subin@zju.edu.cn

Table of Contents

S1. Preparation of ITO electrode-supported and perforated SNM

S2. Characterization of Pt UME

S3. SNM characterization

S4. CV of $\text{Ru}(\text{CN})_6^{4-}$ at Pt UME

S5. COMSOL Multiphysics simulation

S2. Characterization of Pt UME

The Pt UME tip of a $\sim 5 \mu\text{m}$ radius with an $RG \approx 3$ was always polished prior to use. The polished tip was then characterized by cyclic voltammetry and SECM approach curve in a 1 mM FcMeOH aqueous solution containing 1 M KCl. The tip with a smooth surface gave rise to a sigmoidal steady-state cyclic voltammogram with a small capacitive current (see **Figure S1a**). Assuming a disk-shaped geometry, the limiting current $i_{T,\infty}$ at the tip is given by the following equation, namely **eq. 1** in the manuscript,

$$i_{T,\infty} = 4nFDac \quad (1)$$

where n is the number of electrons transferred in the tip reaction, F is the Faraday constant, c is the bulk concentration, D is the diffusion coefficient and a is the tip radius.

The characterization of tip was also performed by approaching the tip to a 5 mm-radius Pt disk electrode surface. The tip current in the approach curves was normalized with respect to $i_{T,\infty}$ in the bulk solution. As shown in **Figure S1b**, the tip current can increase to 700 % of $i_{T,\infty}$ upon approaching. The result confirms that the glass orifice of tip can be brought very close to the electrode surface. The theoretical fitting of approach curve yielded $a = 5 \mu\text{m}$ and $RG = 3$. **Figure S1c** shows the metallograph of the Pt tip surface that also confirms a smooth surface and the tip size.

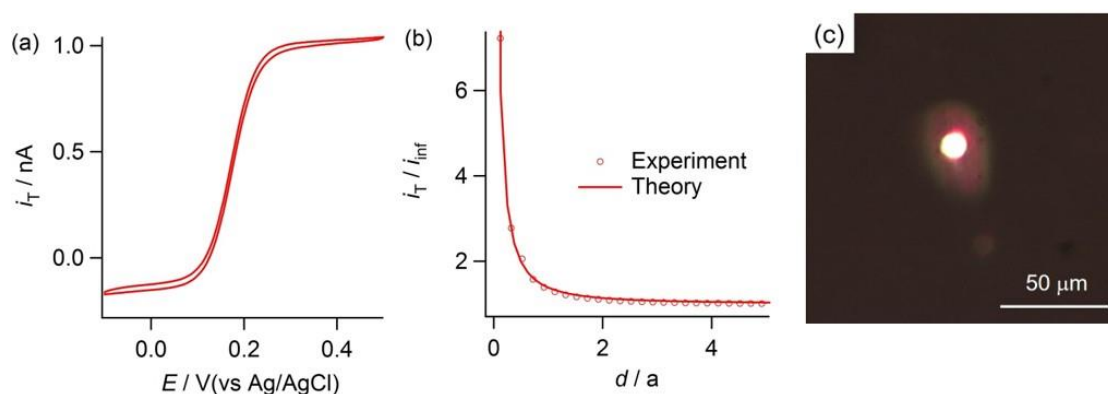


Figure S1. (a) Voltammetric response for the oxidation of 1 mM FcMeOH in 1 M KCl solution. The potential was scanned from -0.1 V to 0.5 V at a rate of 10 mV/s. (b) SECM approach curve obtained by approaching to Pt disk substrate in a solution containing 1 mM FcMeOH and 1 M KCl. The tip potential was kept at $+0.5$ V vs Ag/AgCl. The maximum tip approach rate was $50 \mu\text{m/s}$. (c) Metallograph of the tip surface of Pt UME.

S3. SNM characterization

As-prepared SNM/ITO electrode was characterized by electrochemical methods. $\text{Ru}(\text{NH}_3)_6^{3+}$ and $\text{Fe}(\text{CN})_6^{3-}$ were used as probe molecules. When CTAB micelles were retained in nanochannels (I of **Scheme S1**), no faradic currents were observed for both. After CTAB removal (II of **Scheme S1**), obvious current peaks were obtained, indicating the SNM on ITO surface was compact without cracks or leakages. Moreover, the peak current of $\text{Ru}(\text{NH}_3)_6^{3+}$ is apparently much larger than that of $\text{Fe}(\text{CN})_6^{3-}$, suggesting the permselectivity of SNM towards cations. Given silica nanochannels are negatively charged, the permeation of cations is preferentially favored. While that of anions is hindered, and the extent of hinderance is dependent on the electrolyte concentration.

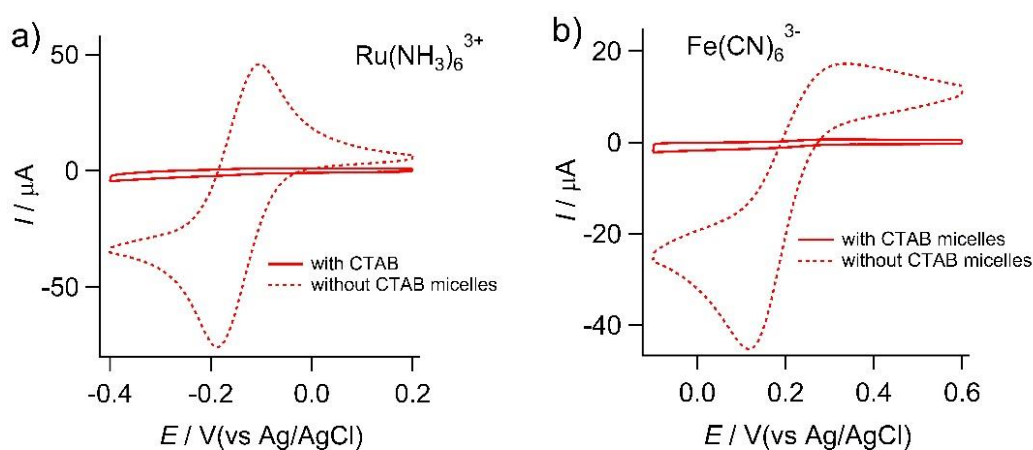


Figure S2. Cyclic voltammetry of CTAB@SNM/ITO and SNM/ITO electrodes in 50 mM potassium hydrogen phthalate (KHP, pH = 4.0) containing different redox probes: (a) 0.5 mM $\text{Ru}(\text{NH}_3)_6^{3+}$. (b) 0.5 mM $\text{Fe}(\text{CN})_6^{3-}$.

The SNM was scraped from the ITO electrode surface, dispersed in ethanol and then dropped onto copper grids for TEM characterization. **Figure S3a** shows the distribution of pore diameter size determined from the top-view TEM image displayed in **Figure 1b**. The distribution was determined using a fractional membrane area of $50 \text{ nm} \times 50 \text{ nm}$ including 100 pores, thereby yielding an average pore radius of 1.15 nm and a pore density of 4×10^{12} pores/ cm^2 (16.7 % in porosity).

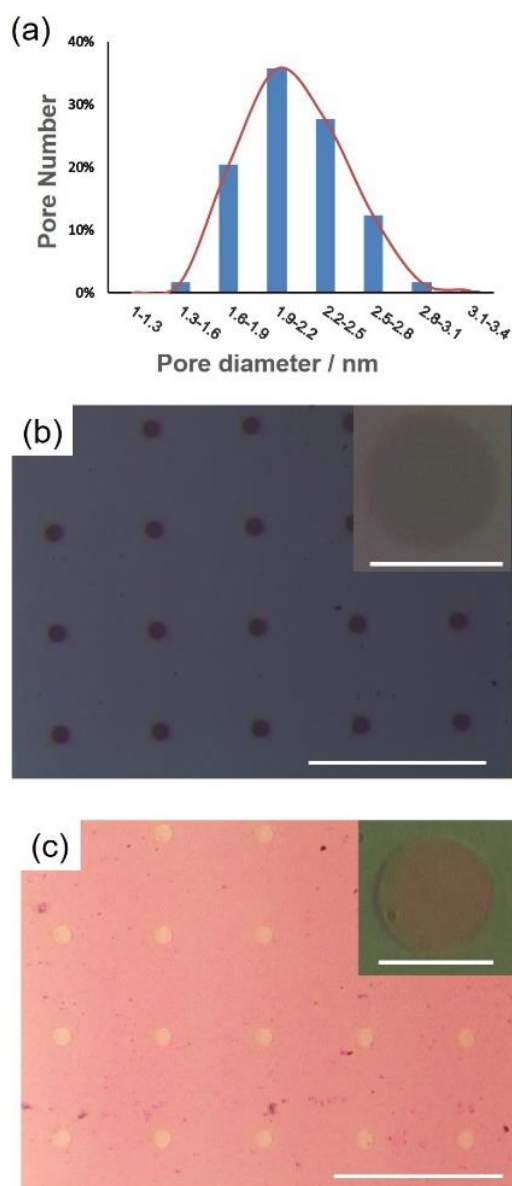


Figure S3. (a) The distribution of nanopore diameter measured from top-view TEM images shown in **Figure 1b**. (b, c) Metallographs of the SiN chip window before (b) and after (c) supporting SNM membrane. The scale bar is 100 μm. The insets show a single micrometer pore before (b) and after (c) supporting SNM transfer with a scale bar of 10 μm.

Figure S3b, c shows the metallographs of the SiN chip window before and after supporting the SNM. In both cases, the array of 10-μm-diameter SiN pores with a pore-to-pore distance of 60 μm can be clearly seen. While after supporting the SNM, the pores are still visible due to the ultrathin thickness of SNM. Moreover, no any visible crack was found in the SNM transferred to the SiN chip. After supporting SNM, the color of chip also changed.

S4. CV of $\text{K}_4\text{Ru}(\text{CN})_6$ at Pt UME

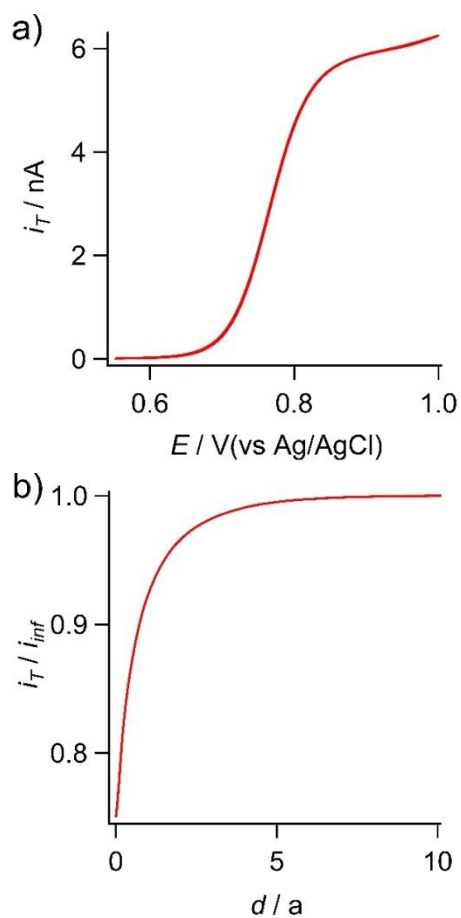


Figure S4. (a) Voltammetric response for the oxidation of 5 mM $\text{Ru}(\text{CN})_6^{4-}$ in 1 M KCl solution. The UME potential was scanned from +0.45 V to +0.95V at a rate of 10 mV s^{-1} . (b) Dimensionless approach curve obtained upon approaching to silicon wafer substrate in the solution containing 5 mM $\text{Ru}(\text{CN})_6^{4-}$. The tip potential was kept at +0.95 V vs Ag/AgCl. The maximum approaching speed was $50 \mu\text{m/s}$.

S5. COMSOL Multiphysics simulation

The steady-state diffusion of $\text{Ru}(\text{CN})_6^{4-}$ through SNM and the electrical double layer (EDL) were simulated using COMSOL Multiphysics (version 5.2).

S5.1. Simulation of $\text{Ru}(\text{CN})_6^{4-}$ diffusion through SNM

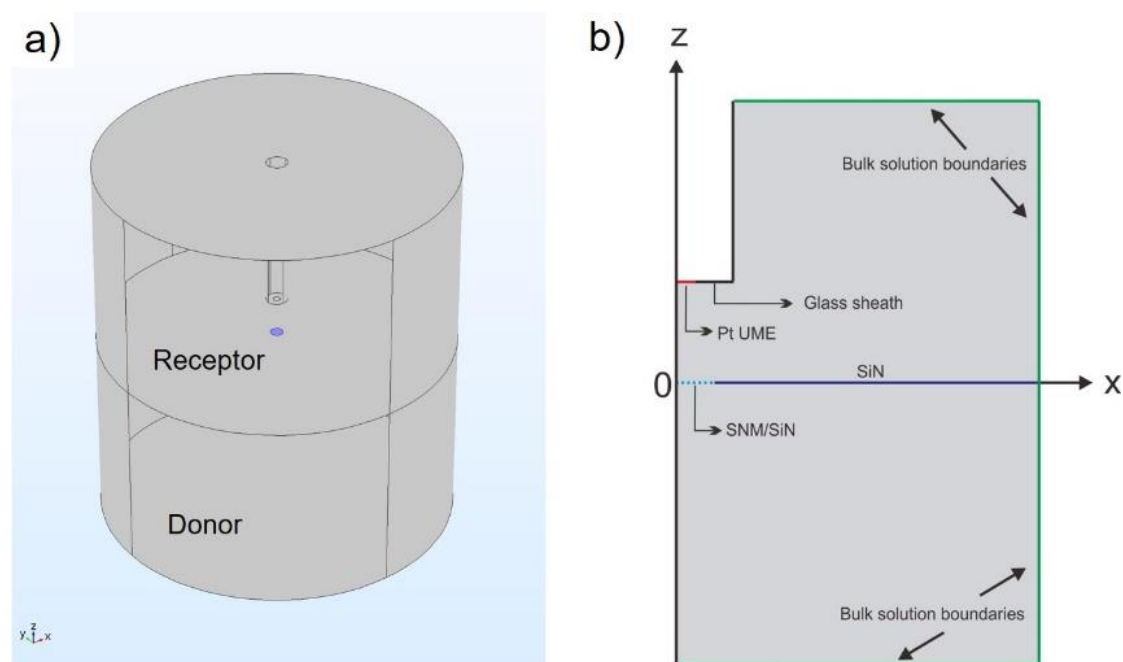


Figure S5. a) Three-dimensional (3D) model geometry of the SECM tip approaching a single SiN pore covered with SNM. b) Two-dimensional (2D) view in the x - z plane with labeled boundaries.

In the $\text{Ru}(\text{CN})_6^{4-}$ diffusion simulation, a 3D model was built in Cartesian coordinates, as shown in **Figure S5a**, to simulate the same physical geometry as the SECM experiments. The Pt UME geometry was defined according to the characterization results mentioned above ($5\ \mu\text{m}$ in radius, $R_C = 3$). Considering the high porosity (16.7%), the SNM/SiN was treated as a uniform membrane in this model. As the thickness of SNM (90 nm) was much smaller than the SiN pore diameter ($18\ \mu\text{m}$), the SNM/SiN pore was defined as a circle (marked as blue in **Figure S5a**) instead of a cylinder. The model is defined with two separate domains, representing the donor and receptor compartment in the SECM experiments and each with their own geometry and physics. The initial concentrations of donor and receptor domain were specified as $c_{d,0} = 5\ \text{mM}$, $c_{r,0} = 0\ \text{mM}$ or $5\ \text{mM}$. In both

domains, the bulk solution boundaries (green lines in **Figure S5b**) were defined to be 500× of the Pt UME radius away from the pore center ($x, y, z = 0 \mu\text{m}$) and the concentration for these boundaries were set as the initial concentrations, $c_{d,0}$ and $c_{r,0}$, respectively.

The diffusion of $\text{Ru}(\text{CN})_6^{4-}$ in both donor and receptor solutions is defined by the Fick's second law,

$$\frac{\partial c_d(x, y, z)}{\partial t} = D \left[\frac{\partial^2 c_d(x, y, z)}{\partial x^2} + \frac{\partial^2 c_d(x, y, z)}{\partial y^2} + \frac{\partial^2 c_d(x, y, z)}{\partial z^2} \right] \quad (\text{S1})$$

$$\frac{\partial c_r(x, y, z)}{\partial t} = D \left[\frac{\partial^2 c_r(x, y, z)}{\partial x^2} + \frac{\partial^2 c_r(x, y, z)}{\partial y^2} + \frac{\partial^2 c_r(x, y, z)}{\partial z^2} \right] \quad (\text{S2})$$

where c_d and c_r are the concentrations of $\text{Ru}(\text{CN})_6^{4-}$ in the donor and receptor solutions, respectively. D is the diffusion coefficient of $\text{Ru}(\text{CN})_6^{4-}$.

The boundary condition of the SNM/SiN pore was given by,

$$D \left[\frac{\partial c_d(x, y, z)}{\partial x} \right]_{z=0} = D \left[\frac{\partial c_r(x, y, z)}{\partial x} \right]_{z=0} = P \times [c_d(x, y, 0) - c_r(x, y, 0)] \quad (\text{S3})$$

where P is the permeability of SNM.

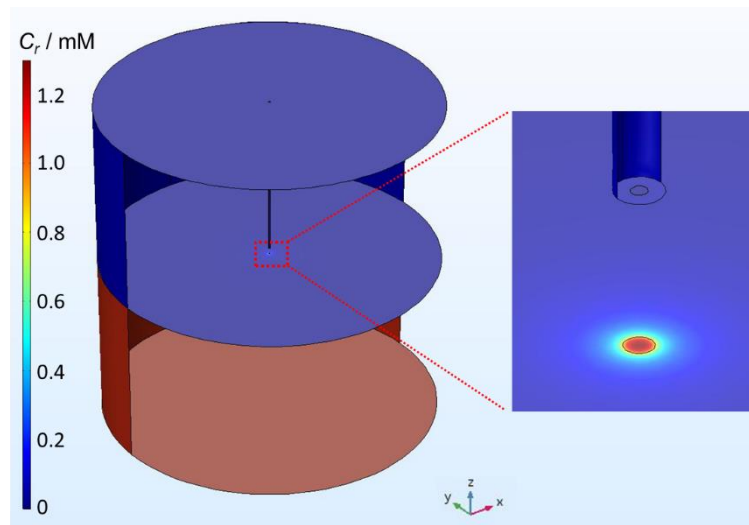


Figure S6. Surface concentration map of the donor and receptor bulk solution domain with the area near the tip and pore surface zoomed in.

The permeability simulation was solved by the one-step stationary study. The Pt UME was biased and approached to the SNM/SiN pore, generating concentration profiles for each tip-pore distance (**Figure S6**). Parameterizing the tip-pore distance (z -axis) and permeability allowed the automated simulation of a single SECM approach curve experiment, which could generate a series of approach curves after a single simulation run.

The tip current was measured from the concentration profile at each tip position, which was obtained by integrating the flux of $\text{Ru}(\text{CN})_6^{4-}$ to the Pt surface. The current can be described by the following equation,

$$i = 2\pi nFD \int_0^a r \left[\frac{\partial c_r(r, z, t)}{\partial z} \right] dr \quad (\text{S4})$$

where n is the number of electrons transferred in the tip reaction, F is the Faraday constant, D is the diffusion coefficient of $\text{Ru}(\text{CN})_6^{4-}$ ($6.3 \times 10^{-10} \text{ m}^2/\text{s}$) and a is the tip radius ($5 \mu\text{m}$).

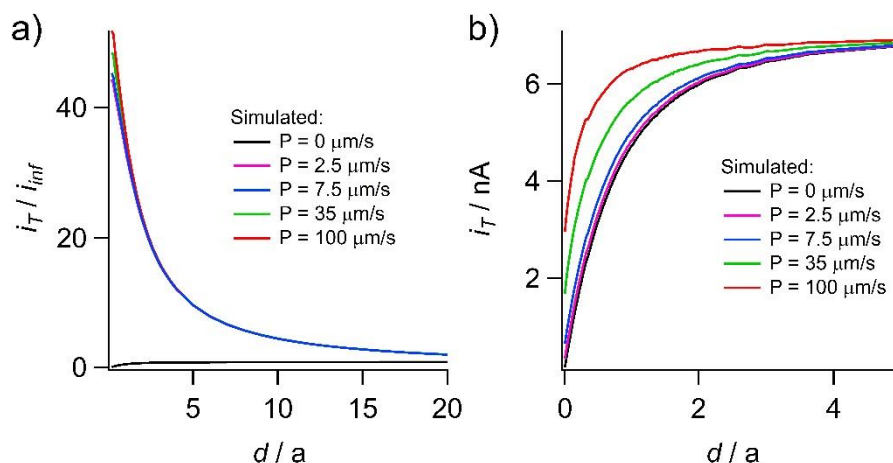


Figure S7. a) Simulated dimensionless approach curves to a single SNM/SiN pore without addition of 5 mM $\text{Ru}(\text{CN})_6^{4-}$ to the receptor solution. b) Simulated tip current as a function of normalized tip-pore separation with addition of 5 mM $\text{Ru}(\text{CN})_6^{4-}$ to the receptor solution.

Figure S7a shows the simulated dimensionless approach curves (the tip current normalized by the current far from substrate) to a single SNM/SiN pore without addition of 5 mM $\text{Ru}(\text{CN})_6^{4-}$ to the receptor solution. At different membrane

permeabilities, the approach curves remain the same until the tip approaches to a very small tip-pore distance, which precludes the proper curve fittings. As a result, in this case, the tip current is directly plotted versus tip-pore distance without further normalization. Nevertheless, in the case of adding 5 mM $\text{Ru}(\text{CN})_6^{4-}$ initially, there is no difference in approach curve shape between normalized and unnormalized ones.

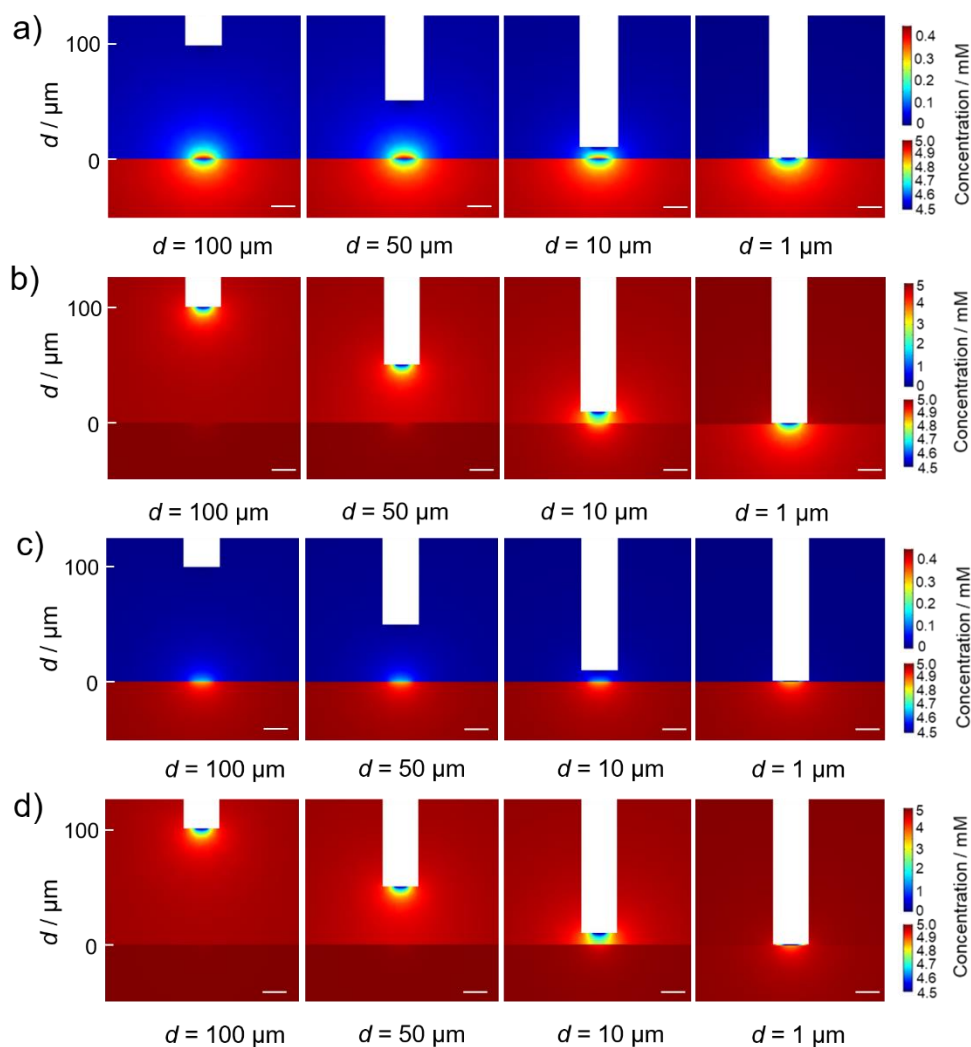
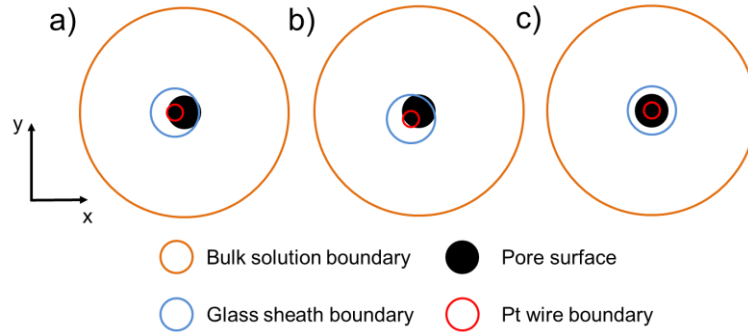


Figure S8. Vertical views of simulated concentration profiles of $\text{Ru}(\text{CN})_6^{4-}$ in the receptor and donor solutions at different d (annotated below each image) at a membrane permeability of $7.5 \mu\text{m/s}$ (a,b) and $2.5 \mu\text{m/s}$ (c,d) for two cases: no $\text{Ru}(\text{CN})_6^{4-}$ (a,c) or 5 mM $\text{Ru}(\text{CN})_6^{4-}$ (b,d) initial addition to the receptor solution. In the simulation, the x and y position of the tip was always kept at 0. The color legends denoting the receptor and donor concentrations of $\text{Ru}(\text{CN})_6^{4-}$ were set differently to better reveal the concentration profiles. The scale bar in each image represents the displacement of $20 \mu\text{m}$ in the x direction.



Scheme S2. Schematic of relative positions between the centers of the tip and pore in x and y directions for the simulation at x - y plane view. a) $\Delta y = 0$, $\Delta x = -5 \mu\text{m}$; b) $\Delta y = -5$, $\Delta x = -5 \mu\text{m}$ and c) $\Delta y = 0$, $\Delta x = 0 \mu\text{m}$. Δy and Δx are defined as the distance between the center of the tip and the center of pore ($x, y, z = 0 \mu\text{m}$) in x - and y -direction, respectively. The tip-pore distance in z direction is set to $5 \mu\text{m}$. The orange, blue and red circles represent the boundary of bulk solution, outer boundary of the glass sheath around the Pt wire and outer boundary of the Pt wire, respectively. The SNM/SiN is represented by a black cycle.

The effect of tip position on the approach curve was also assessed by COMSOL Multiphysics simulation. The same model as abovementioned was built except for the variation of tip position. In this model, the position of the SNM/SiN pore (black cycle in **Scheme S2**) is kept at $x, y, z = 0 \mu\text{m}$. The lateral distance of the tip center from the pore center is defined as Δx in x direction and Δy in y direction. In **Scheme S2a**, the tip center is $5 \mu\text{m}$ away from the pore center only in x direction ($\Delta x = -5$, $\Delta y = 0 \mu\text{m}$). In **Scheme S2b**, the tip center is $5 \mu\text{m}$ away from the pore center in both x and y directions ($\Delta x = -5$, $\Delta y = -5 \mu\text{m}$). In **Scheme S2c**, the center of the tip and pore is perfectly aligned in both x and y directions ($\Delta x = 0$, $\Delta y = 0 \mu\text{m}$). Approach curves for three different tip positions could be generated from simulation results (**Figure 6d**).

S5.2. Simulation of EDL

At the electrode-electrolyte interface, there is a thin layer of space charges, called the diffuse double layer. When SNM contacts an aqueous solution including electrolyte, the surface of silica nanochannel wall becomes negatively charged due to deprotonated silanol groups. The surface charges cause a special structure at the interface, the so-called electrical double layer (EDL). In this region, electroneutrality does not hold.

Here the Gouy-Chapman-Stern model is used to describe the structure of EDL (**Figure 5a**). In this model, the EDL consists of two layers, namely Stern layer and diffuse layer. Stern layer is the region closest to the wall surface, where the specific adsorption of solvent molecules and ions occurs. The locus of electrical centers of the specifically adsorbed ions is called the inner Helmholtz plane (IHP, black dotted line in **Figure 5a**). The locus of centers of these nearest solvated ions is called the and the outer Helmholtz plane (OHP, green dotted line in **Figure 5a**). The diffuse layer is the region next to the Stern layer, where ions can move freely in any direction. The thickness of the diffuse layer depends on the total ionic concentration in the solution, which is determined by COMSOL Multiphysics (see below). The radial potential profile across the EDL in a nanochannel can be expressed by the Poisson-Boltzmann equation in the cylindrical coordinate for a symmetrical electrolyte (e.g., KCl),³

$$\frac{d^2\phi}{dr^2} + \frac{1}{r} \frac{d\phi}{dr} = \frac{2n_0e}{\epsilon_0\epsilon_r} \sinh\left(\frac{e\phi}{kT}\right) \quad (\text{S5})$$

where ϕ is measured with respect to the bulk solution. n_0 , e , ϵ_0 , ϵ_r , k and T are the bulk concentration, the electron charge, the permittivity of free space, relative dielectric constant of the solution, the Boltzmann constant and the absolute temperature, respectively.

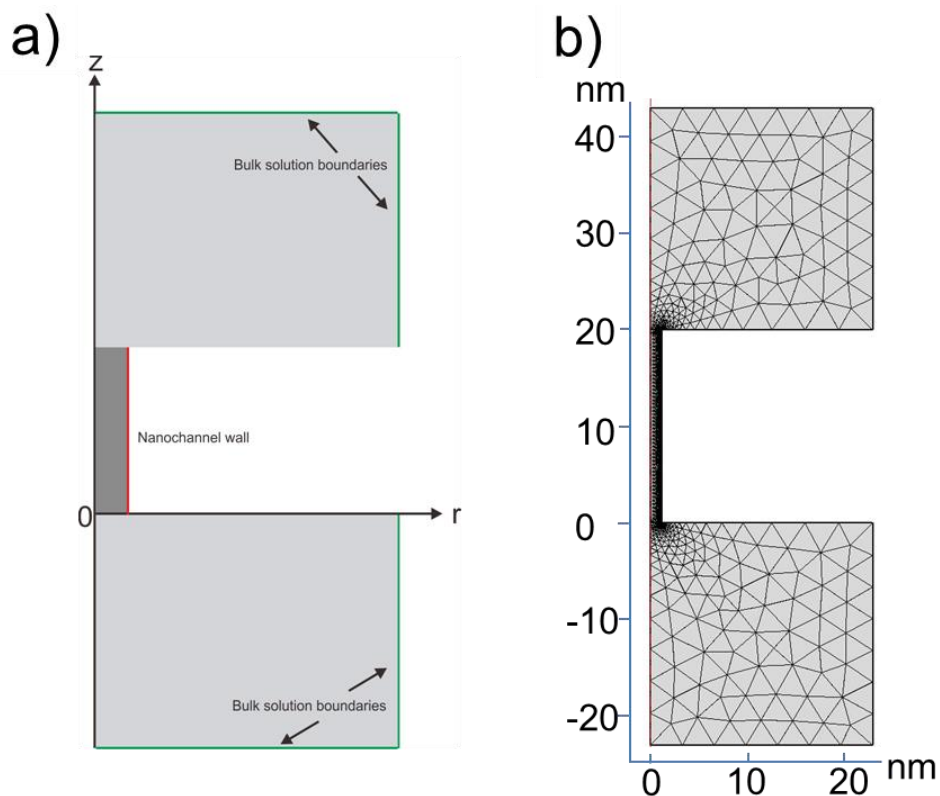


Figure S9. a) Two-dimensional symmetric model employed in the EDL simulation. b) Meshed 2D model.

In EDL simulation, a 2D symmetric model with a single nanochannel of SNM connecting to two large reservoirs was employed, as shown in **Figure S8a**. Considering the length of nanochannel has no effect on the potential distribution in EDL along pore radius the length of the nanochannel was set to 20 nm instead of its real length of 90 nm to reduce the computation time. The dimensions of the two large reservoirs were defined to be 20× of the nanopore radius away from the symmetric axis ($r = 0$ nm). The built model was then meshed using a free triangular mesh (**Figure S8b**). As the size of the mesh is directly related to the accuracy of the finite element analysis simulation, the discretization near the charged wall should be specifically considered. Here a discretization length scale of 1/100 times the Debye length ($1/\kappa$; see **Eq S9** for the definition of κ) was used to accurately resolve the abrupt change in the EDL.

Two physical modules are involved in this simulation, Electrostatics and Transport of Diluted Species. The electrostatics physics contains the equations, boundary conditions and space charge densities for solving the electric potential. The space charge densities for all the three domains are defined as,

$$F*(C_c - C_a) \quad (S6)$$

where F is the Faraday constant, C_c and C_a are the concentrations of cations and anions, respectively.

The concentration of cations and anions were computed by the Transport of Diluted Species interface. At the bulk solution boundary (denoted with green lines in **Figure S8a**), the electrolyte potential was set as ground. The boundary condition for the nanochannel wall (denoted with red line in **Figure S8a**) is defined by surface charge density. According to Gouy-Chapman-Stern model, the surface charge density on the nanochannel wall depends on the potential difference between the electrode potential (ϕ_0) and the potential at the outer Helmholtz plane (ϕ). The potential difference can be defined by following equations,

$$\Delta\phi = \phi_0 - \phi \quad (S7)$$

$$\rho_s = \varepsilon_0 \varepsilon_r \kappa \Delta\phi \frac{I_1(\kappa a)}{I_0(\kappa r)} \quad (S8)$$

$$\kappa = \sqrt{\frac{2F^2 c_0}{\varepsilon_0 \varepsilon_r RT}} \quad (S9)$$

where c_0 is the bulk concentration of electrolyte in mol/m³, R is the gas constant, F is the Faraday constant and a is the radius of the nanochannel. r is the distance from the axial center of nanochannel. I_0 and I_1 are the zero and first order modified Bessel functions of the first kind, respectively.

The Transport of Diluted Species interface solves the concentrations of cation and anion. Two transport mechanisms were involved, namely diffusion (Fick's law) and migration in

electric field (the electrical field is computed by the Electrostatics interface). For bulk boundary condition, the concentrations of cation and anion were set the same to match the Poisson-Boltzmann equation.

References

1. Teng, Z.; Zheng, G.; Dou, Y.; Li, W.; Mou, C. Y.; Zhang, X.; Asiri, A. M.; Zhao, D., Highly ordered mesoporous silica films with perpendicular mesochannels by a simple stöber-solution growth approach. *Angewandte Chemie - International Edition* **2012**, *51* (9), 2173-2177.
2. Lin, X. Y.; Yang, Q.; Ding, L. H.; Su, B., Ultrathin Silica Membranes with Highly Ordered and Perpendicular Nanochannels for Precise and Fast Molecular Separation. *ACS Nano* **2015**, *9* (11), 11266-11277.
3. Yang, Q.; Lin, X.; Wang, Y.; Su, B., Nanochannels as molecular check valves. *Nanoscale* **2017**, *9* (46), 18523-18528.